A Three-Dimensional Simulation of the Hudson–Raritan Estuary. Part I: Description of the Model and Model Simulations

LIE-YAUW OEY* AND GEORGE L. MELLOR

Geophysical Fluid Dynamics Program, James Forrestal Campus, Princeton University, Princeton, NJ 08542

RICHARD I. HIRES

Department of Civil and Ocean Engineering, Stevens Institute of Technology, Hoboken, NJ 07030

(Manuscript received 12 December 1984, in final form 31 May 1985)

ABSTRACT

A time-dependent, three-dimensional, finite difference simulation of the Hudson–Raritan estuary is presented. The calculation covers July–September 1980. The model estuary is forced by time-dependent observed winds, tidal elevation at open boundaries, and river and sewage discharges. Turbulence mixing coefficients in the estuary are calculated according to a second-moment, turbulence-closure submodel. Horizontal diffusivities are zero in the simulation and small-scale eddies produced by the interaction of unsteady, three-dimensional velocity and salinity fields with coastline and bottom bathymetry were resolved by the model. These eddies are important physical elements in shear dispersion processes in an estuary.

Model results show unstably stratified water columns produced by advection of waters of different densities. These instabilities produce intense mixing with vertical eddy diffusivities reaching 2–3 times their neutral values. They occur most frequently at slack currents, during initial stages of flooding currents and also during up-estuary wind events. These three-dimensional, time-dependent solutions extend previous analytical model results and are consistent with observations in partially mixed and well mixed estuaries.

Model results show large subtidal response of velocity and salinity fields to wind forcing. Wind forcing modifies the density-induced flows in deep channels in the estuary and also the horizontal circulation in Raritan Bay where the average water depth is less than 5 m and tidal currents are weak.

1. Introduction

Analytical modeling of estuarine hydrodynamics usually requires simplifying assumptions such as steady state or an ideal estuarine geometry (Hansen and Rattray, 1965; Chatwin, 1976; Hamrick, 1979; and Oey, 1984). A real estuary is never in a steady state, however, and its coastline geometry and bottom topography are usually complicated. It is generally not possible to single out one or two preferred scales that can be used to simplify the governing equations. Numerical models such as those given by Hamilton (1975), Festa and Hansen (1976), Caponi (1976), Johns (1978), Leendertse and Liu (1977), Tee (1979), Owen (1980), Oey *et al.* (1985a; henceforth referred to as OMH) and Sundermann and Lentz (1983) offer certain advantages in that one can cope with more realistic physical inputs than is otherwise possible. Depth-integrated xy-models or width-averaged xz-models lack generality, however, as they do not simultaneously cope with significant vertical variations in salinity and velocity and with complex coastline geometry and often require adjustments of model constants to fit observations. Tee (1979) used a linear set of equations and separated the vertical deviations of the currents from their vertical averages. He was only interested in three-dimensional tidal currents, however, and did not consider vertical and horizontal salinity variations. Owen (1980) used a Galerkin method in the vertical and a finite difference grid in the horizontal to compute three-dimensional tidal currents in Bristol Bay, England. Again, no stratification effects were considered. These models use algebraic eddy diffusivity expressions that are adjusted to fit observations. Earlier three-dimensional models that include density variations were given by Caponi (1976) and Leendertse and Liu (1977) for Chesapeake Bay, San Francisco Bay and Alaskan coastal waters. These models were restricted by insufficient computer time and storage, however, and used such coarse grid sizes that unrealistically large horizontal diffusion terms were needed, either to damp out numerical oscillations or to account for Taylor's (1954) shear dispersion. Moreover, the viability of the baroclinic portion of these models, which determines the important salt balance in an estuary, for example, has never been firmly established, as only simulations of a few days duration have been conducted.

* Present Affiliation: Skidaway Institute of Oceanography, Savannah, GA 31416.

In this paper, we present some results of a real-time, three-dimensional numerical simulation of the Hudson–Raritan estuary for the period covering July–September 1980, corresponding to a period of low river discharge and for which there are velocity and salinity measurements. The simulation is carried out on a supercomputer, which enables us to use fine grid sizes to account for horizontal dispersion processes due to small-scale advection and vertical mixing (Taylor, 1954); the model's horizontal diffusivities are set to zero. Vertical turbulence mixing coefficients are calculated according to a second-moment, turbulence-closure submodel without any adjustment of the model constants.

The Hudson–Raritan estuary is a drowned-river, partially mixed estuary located on the northeast coast of the United States (40°31'N, 74°W; Fig. 1). The major source of freshwater discharge is the Hudson River, with monthly average discharges ranging from about 100 $m^3 s^{-1}$ in dry seasons to about 1800 $m^3 s^{-1}$ in spring. The combined monthly average discharge of Raritan, Hackensack, and Passaic rivers ranges from 10 to 100 $m^3 s^{-1}$. The estuary is connected to the Atlantic Ocean through the Sandy Hook–Rockaway Point transect (henceforth the SHRP transect) toward the southeast and to Long Island Sound through the East River strait toward the northeast. These are open boundaries where we shall specify sea level elevations and salinity distributions. Another important factor that governs the circulation in the estuary is the surface wind stress. Our model also includes this as part of the surface boundary conditions.

The purpose of the present research is (i) to study the mixing processes, the velocity and salinity structures in the estuary, and to understand how these structures are affected by transient winds and different tidal ranges; (ii) to test the general predictive capability of a time-dependent, three-dimensional numerical model as it is applied to an estuary with realistic topography, and forced by synoptic sea level, winds and river discharges; (iii) to study estuarine circulation and salt transport, particularly in relation to winds and other

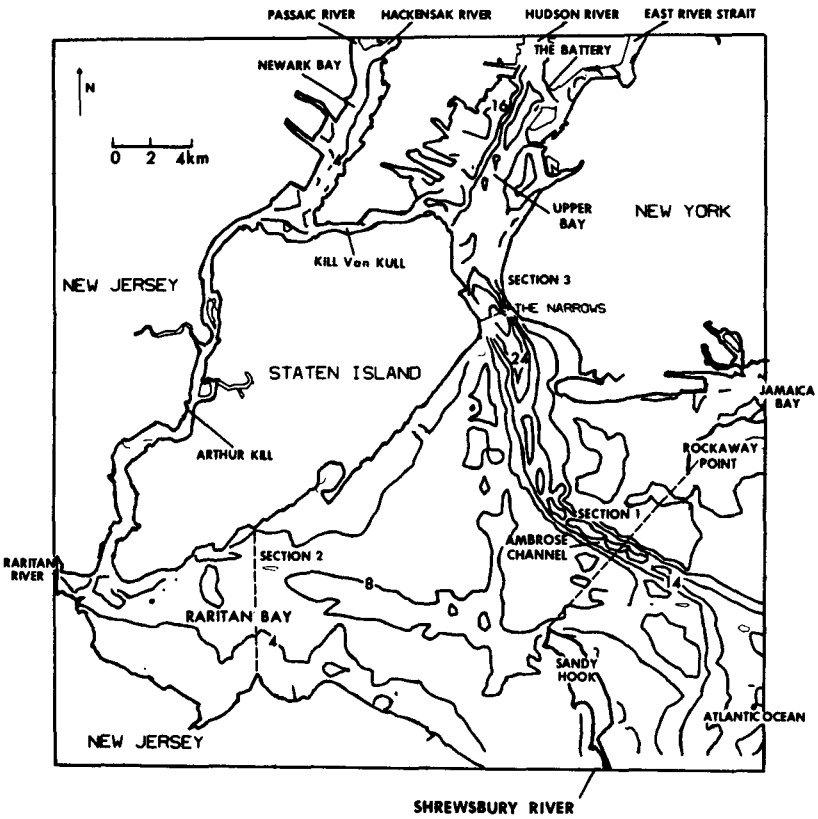

FIG. 1. Location map and computational model region of the Hudson–Raritan estuary. Depth contours are in meters below mean tide level. Rivers are also included in the calculation but they are not shown in the figure in order that we may show greater details of the main estuary. The calculation in East River Strait (shown near the northeastern boundary) ends at Willets Point, some 18 km beyond the northern model boundary of the strait shown here. Jamaica Bay is also included in the model, using the land storage region labeled "New York" in the figure. Details of these implementations are given by Oey *et al.* (1985a).

subtidal forcings; and (iv) to determine the dominant salt dispersion mechanism in the estuary, and to study how the different mechanisms may be related to estuarine geometry, winds, stratification and tides.

This paper is Part I of a series of three papers and contains results we have obtained under item number (i). We shall consider (ii) and (iii) in Part II (Oey *et al.*, 1985b). The results obtained under item number (iv) are in Part III (Oey *et al.*, 1985c).

In addition to the present low freshwater discharge simulation, we have also completed a high discharge calculation. Oey (1984) has used some of these numerical results to check the validity of a generalized Hansen–Rattray theory of salt transport in estuaries.

2. The mathematical model

A detailed description of the numerical algorithm is given by Blumberg and Mellor (1980, 1983). We shall give an outline here. The model responds to tidal forcing, surface winds, and heat and evaporative mass fluxes and solves for elevations and for the three-dimensional velocity and density fields.

The model solves the continuity equation

$$U_x + V_y + W_z = 0 \tag{1}$$

and Reynolds' momentum equations:

$$U_t + (U^2)_x + (UV)_y + (UW)_z - fV = -P_x/\rho_0 - (\overline{uw})_z \tag{2}$$

$$V_t + (UV)_x + (V^2)_y + (VW)_z + fU = -P_y/\rho_0 - (\overline{vw})_z \tag{3}$$

$$\rho g = -P_z \tag{4}$$

where x is positive eastward, y positive northward and z positive upward (the origin at the mean tidal level); t is time; $U + u$, $V + v$ and $W + w$ are instantaneous velocities in the x, y and z directions, respectively, where U, V and W denote the ensemble mean velocities and u, v and w the corresponding fluctuating velocities; $\overline{uw}$ and $\overline{vw}$ are turbulent Reynolds stresses defined by

$$(-\overline{uw}, -\overline{vw}) = K_M(U_z, V_z), \tag{5}$$

where K_M is the turbulence mixing coefficient for momentum to be defined shortly; f is the Coriolis parameter = 9.49×10^{-5} s^{-1}; ρ is the mean density and ρ_0 is a reference density; g is the acceleration due to gravity and P is the pressure. We have made the hydrostatic assumption in (4) and the Bousinesq assumption so that density differences are neglected unless they are multiplied by gravity.

The equation for the mean salinity, S, is

$$S_t + (US)_x + (VS)_y + (WS)_z = -(\overline{ws})_z \tag{6}$$

where the turbulence salt flux $\overline{ws}$ is defined by

$$-\overline{ws} = K_H S_z \tag{7}$$

and K_H is the turbulence mixing coefficient for salt. Equations similar to (6) and (7) for temperature T may also be solved by the model but have been omitted. The density is related to the salinity and temperature by an equation of state (Fofonoff, 1962)

$$\rho = \rho(T, S) \tag{8}$$

where, here, $T = 17$°C.

The coefficients K_M and K_H are calculated according to Mellor and Yamada's (1974, 1982) "level 2.5" turbulence model wherein,

$$K_M = S_M l q, \quad K_H = S_H l q, \tag{9}$$

l is the turbulence length scale and $q^2/2$ is the turbulence kinetic energy. They are calculated from turbulence transport equations of the form

$$DF/Dt = (\text{diffusion of } F) + (\text{shear and buoyancy productions of } F) + (\text{dissipation of } F) \tag{10}$$

where F denotes either $q^2/2$ or $q^2 l$. The S_M and S_H are stability factors which depend on q, l, $U_z^2 + V_z^2$ and $g\rho_z/\rho_0$.

Equations (1)–(10) are cast in finite difference forms and stepped forward in time using a leapfrog time scheme. The scheme is explicit in the advective transport terms and, because of the generally finer mesh spacing in z, is implicit in the vertical diffusive flux terms. It is formally second-order accurate in space and first-order accurate in time. The temporal error cannot be large, however, because of the short time step Δt imposed for stability by the Courant condition of the form

$$\Delta t < \tfrac{1}{2}\,[c^2(1/\Delta x^2 + 1/\Delta y^2)]^{-1/2} \tag{11}$$

where Δx and Δy are grid sizes in the x and y directions and c is the phase speed of either the free surface gravity wave or the internal gravity wave. The model uses the "barotropic-baroclinic" mode-splitting technique. Equations (1)–(4) are vertically integrated and the barotropic set of equations that results is integrated in time with a short time step determined by $c = (gH_{\max})^{1/2}$ in (11), where $H_{\max}$ is the maximum water depth below the mean tidal level. The full three-dimensional set of equations is integrated in time with a larger time step determined by the baroclinic internal-wave speed $c_i \approx (gH_{\max}\delta\rho/\rho)^{1/2}$; where $\delta\rho$ is the top-to-bottom density difference. In our calculation with $\Delta x = \Delta y = 0.53$ km, Δt is 15 sec if c is the surface gravity wave speed and Δt is 3 min if c is the internal-gravity-wave speed; both are much smaller than the M_2 tidal period of 12.42 hours. Thus, for every twelve barotropic calculations, we need only calculate the three-dimensional "baroclinic" set of equations once. The "baroclinic" mode calculation supplies computed

bottom friction and vertical integrals of density and vertical variances of horizontal velocity to the barotropic mode calculation. In turn, the barotropic mode calculation supplies surface elevation to the "baroclinic" mode calculation.

The model uses a "σ" coordinate in the vertical, where

$$\sigma = (z - \eta)/(H + \eta),$$

and where η is the surface elevation and H is the depth below the mean tidal level. Irregular bottom topography and a time-dependent surface elevation are accommodated by the model, simply and accurately. For the present application of the model, there are 11 σ-levels (σ = 0., −0.03125, −0.0625, −0.125, −0.25, −0.5, −0.75, −0.875, −0.9375, −0.96875, −1.).

a. Connections to rivers and Jamaica Bay

For an estuary that consists of broad water regions as well as narrow channels and rivers, it is impractical to model narrow waterways three-dimensionally and they are, therefore, modeled by width-averaged equations as a subset of the full three-dimensional equations (1)–(10). These narrow rivers are stored in computer memory which, otherwise, would correspond to the land areas shown in Fig. 1, and are therefore included at no additional computer cost. The four rivers and one strait handled in this way are the Hudson, Hackensack, Passaic and Raritan rivers and the East River strait. Additional matching conditions are imposed at river–bay junctions.

Jamaica Bay has an average depth of about 3 m and is further complicated by the presence of small islands and marsh areas. These fine details can barely be resolved by our present model resolution. Since the circulation and salinity distribution inside the bay are not of particular interest to us we decided to model the bay with a constant-depth "bay" of approximately equal volume and store it in computer memory in the land area labeled "New York" in Fig. 1. Matching conditions are imposed at the mouth of Jamaica Bay connecting to the main harbor region.

This grid arrangement, in which calculations are made sweeping across a rectangular domain including both "land" (now mostly assigned as "rivers" and "Jamaica Bay") and water regions, are most suitable for vector processing machines. Further details can be found in OMH.

b. Boundary conditions

The boundary conditions at the free surface, $z = \eta(x, y, t)$, are:

$$K_M(U_z, V_z) = (\tau_{0x}, \tau_{0y})$$

$$K_H(S_z) = \dot{S}$$

$$q^2 = \text{constant} \cdot |\tau_0|$$

$$q^2 l = 0$$

$$W = U\eta_x + V\eta_y + \eta_t$$

where $\tau_0 = (\tau_{0x}, \tau_{0y})$ is the wind stress vector and $\dot{S} = S(0)(\dot{E} - \dot{P})/\rho_0$ where $(\dot{E} - \dot{P})$ is the net evaporation minus precipitation surface flux rate and has been set to be zero in the present calculation.

At the bottom the boundary conditions for S, q^2 and $q^2 l$ are similar to those at the surface. For W, we have

$$W = -UH_x - VH_y, \quad z = -H(x, y)$$

and for U and V we match computed solutions with the turbulence law of the wall which extends the computed U and V into the viscous or roughness sublayer where the no-slip condition at the ocean floor is satisfied. Thus,

$$(U, V) \sim ((\overline{wu}, -\overline{wv})/ku_*) \cdot \ln[(H + z)/z_0]$$

$$\text{as} \quad z \to -H,$$

where u_* is the bottom friction velocity, k = 0.40 is von Karman's constant and z_0 is the roughness height. For the results in these papers, z_0 = 0.2 cm. Sensitivity studies show that an increase of z_0 to 1 cm decreases the M_2 tidal amplitudes at Sandy Hook and at the Battery by 3 and 7% of the observed amplitudes, respectively.

At open boundaries, the Sandy Hook connection with the Atlantic Ocean and the East River strait connection with Long Island Sound, sea level elevations are specified using NOS tidal records at Sandy Hook and at Willets Point; here linearized momentum equations are used. Since the actual open boundary on the southeastern region of the model is some 10 km away from Sandy Hook the phase of the tidal record is advanced by 15 min (Swansen, 1976). Figure 2 shows the tidal record used at the Sandy Hook open boundary region. The tide in the estuary is mainly semidiurnal with the ratio of the amplitudes of the four major constituents $(K_1 + O_1)/(M_2 + S_2)$ ranging from about 0.12 at Willets Point to about 0.19 at Sandy Hook. During ebb, salinities at open boundaries are calculated using an "upwind" differenced advection equation. During flood, the salinity is linearly interpolated for a duration of one hour from its (computed) value at the end of ebb to a value of 34‰ along the southeastern open boundary and to 27.3‰ at Willets Point. A depth-independent salinity value specified during flood is obviously an over simplification of the actual physics. Ideally a salinity boundary condition with vertical structure, obtained from field observation, would have been preferred. Such data were not available, however.

Upstream of rivers, freshwater discharge velocities are specified and salinities are set to zero. Freshwater discharges were obtained from the U.S. Geological Survey Water Data Report. The Hudson River con-

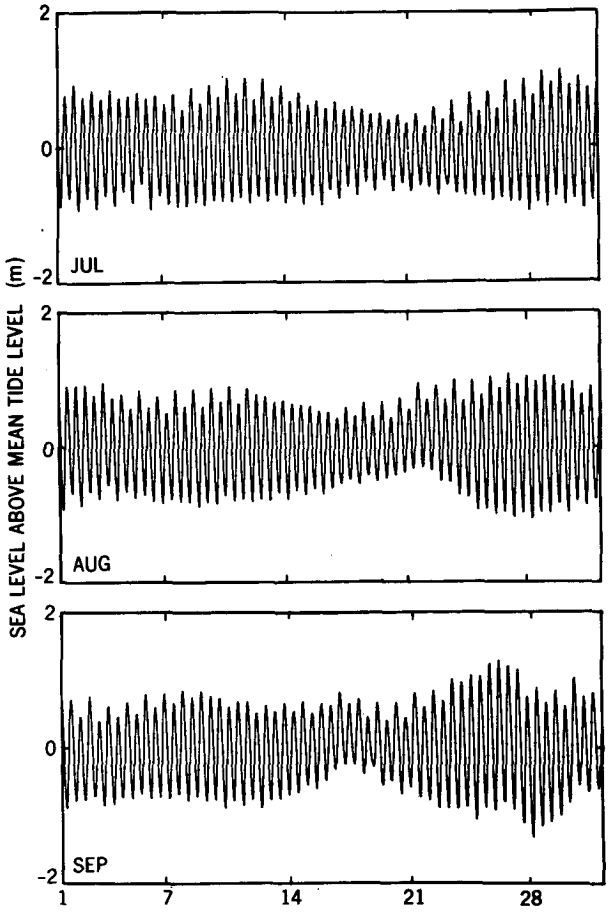

FIG. 2. Tidal elevation record (in meters above mean tide level) at Sandy Hook tide station for July–September, 1980. This record and another one at Willets Point, East River Strait, are used as open ocean boundary conditions in the model.

tributes a mean discharge of 130 $m^3 s^{-1}$ during the simulation period. The Raritan, Passaic and Hackensack river discharges are much smaller with a total mean of 9 $m^3 s^{-1}$. There are four major sewage sources. Two with a combined mean discharge of 11 $m^3 s^{-1}$ are near the mouth of the Passaic River and near the mouth of Kill van Kull, which opens to the upper bay. A third is in the East River with a mean discharge of 42 $m^3 s^{-1}$, and the fourth sewage source is in Jamaica Bay with a mean discharge of 14 $m^3 s^{-1}$. All of these are included as "freshwater" model inputs.

A wind record for the simulation period was obtained from John F. Kennedy International (JFK) Airport, New York, and is assumed spatially uniform for the entire estuary. The wind is generally from the southwest with speeds rarely exceeding 10 m s^{-1} (maximum wind stress $\approx$ 1.5 dyn cm^{-2}). Wind stress components are computed using a wind velocity-dependent drag coefficient (Bunker, 1976) and are shown in Fig. 3.

c. *Initial conditions*

The calculation was initialized with a zero salinity value in each of the rivers and with a transition layer of length of 5 km near its mouth so that salinity values joined smoothly to ocean values in the main harbor; the latter were specified linear in z with 33‰ at the surface and 34‰ at the bottom. The model was spun up from this initial state for 155 days. Freshwater discharges, wind stresses and open ocean sea levels during this spinup period were specified cyclicly every 31 days with values corresponding to July 1980. A water parcel would have traveled the entire length of the Hudson River and into the Atlantic Ocean during this spinup period. Oey (1984) has shown that this spinup time is sufficient for the salt content in the estuary to reach a near-equilibrium state independent of the initial salinity distributions. The model was run for another 61 days to cover August and September 1980. The entire 216 day run required about 20 hours on a CDC-Cyber 205 computer, 15% of which was spent on writing computed results on tapes. With more specialized vector programmings, another doubling in speed is possible but the model would become machine-dependent and not easily transferable to other computers.

3. Computed results

a. *Tidal cycle*

Figure 4 shows four instances of near-surface and near-bottom (1 meter from the bottom) velocity vector and salinity contour plots at 3-hour intervals starting with slack currents at the Narrows. The phasing of the current vector throughout an M_2 tidal cycle agrees with NOS Tidal Current Charts and also with our simpler two-dimensional barotropic calculation (OMH). Vertical velocity shears are significant, however, and salinity contours are of two types. One type of salinity distribution is smooth and occurs in Raritan Bay where the bottom bathymetry and coastline are relatively smooth. Another type shows formation of patches of waters of different salinities and occurs across the SHRP transect, through the Narrows and into the upper bay region south of the Battery. The size of a patch is typically of the order of 9 km^2 (36 grid points) and is therefore well resolved by the model. The life time of each patch is of the order of a few hours or less (time scale of vertical mixing is H^2/K_H, $H \approx 10$ m, $K_H \approx 0.01$ $m^2 s^{-1}$), suggesting that each patch is formed by horizontal advection and subsequent vertical turbulent mixing, i.e., by shear dispersion processes. This dispersion process is important in determining the circulation and salt distribution in an estuary and cannot be simulated well by numerical models with coarse grid resolution. A particular process of mixing that we shall find from both observation and model results oc-

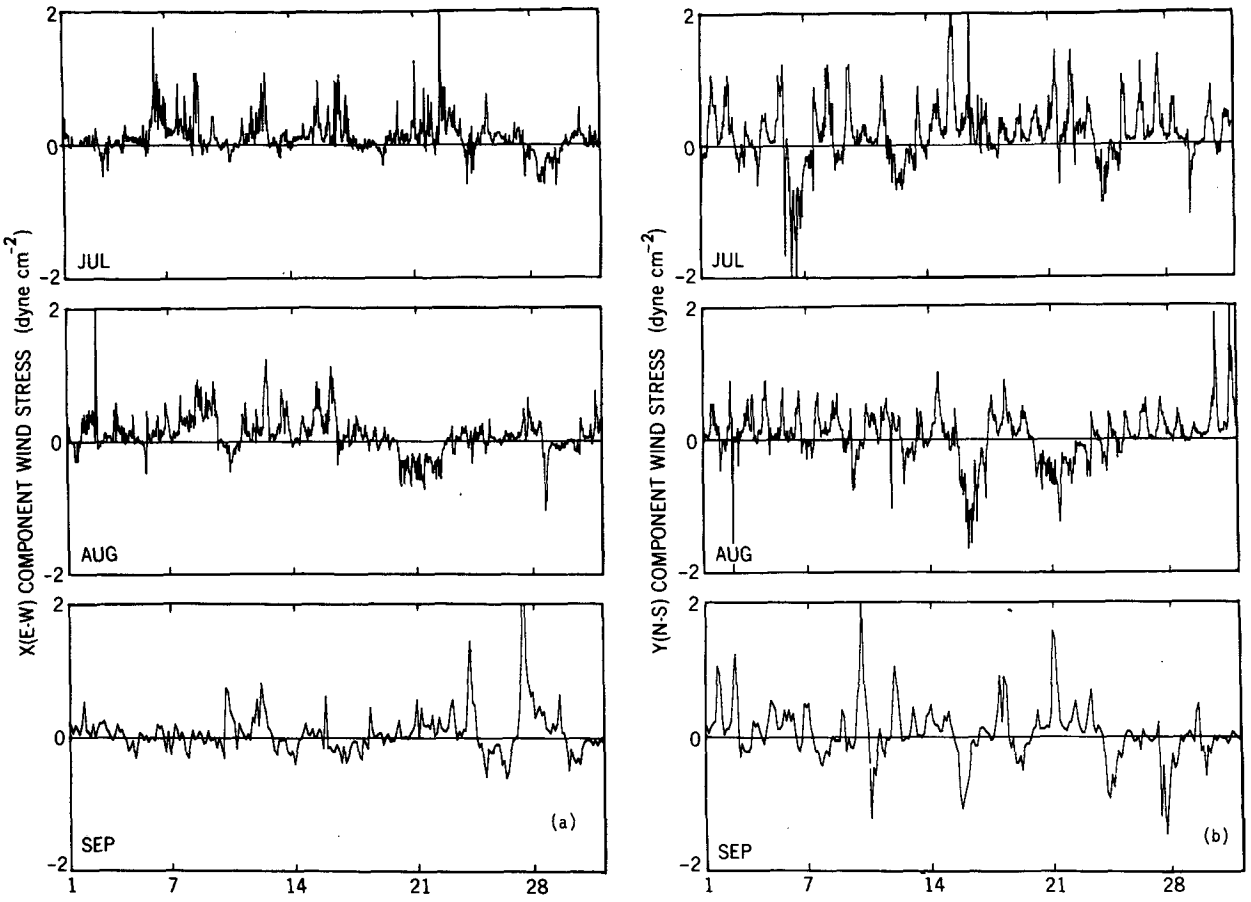

FIG. 3. Wind stresses (dyn cm^{-2}, positive eastward and northward) at JFK airport for July–September 1980: (a) east–west component; (b) north–south component. In the calculation these wind stresses are assumed uniform spatially for the entire modeled region.

curs when two fluids of different salinities converge near the tip of Rockaway Point Peninsula where intense mixing occurs. This is seen in Fig. 4 as the sewage plume from Jamaica Bay mixes with the main harbor's water. This interaction between main harbor water with waters from smaller embayments turns out to be important in the balance of salt at the SHRP transect (see Part III).

In Raritan Bay, the Coriolis effect is such that less-saline water is on the right-hand bank, looking seaward, and the salinity contours resemble surface salinity observations made by Ayers *et al.* (1949).

Salinity distributions depend strongly on the three-dimensional velocity fields. The most notable example occurs in Ambrose Channel running through the mid-section of the SHRP transect and into the Narrows. In Fig. 4a one sees the 30–31‰ contours carried by the previous ebb into the SHRP transect region, and in Fig. 4c these contours are carried by flooding currents into the region just south of the Narrows. Owing to density gradients the salinity intrusion during flood is more extensive near the bottom of the channel (Fig. 4c).

b. Subtidal wind forcing events

Circulation and sea level in the estuary are correlated with winds at time scales of a few days to weeks (Parts II and III). Figure 5 shows some examples of subtidal wind response of velocity and salinity from 15 through 22 August. On 15 August (Fig. 5a), winds were eastward and weak ($\approx$0.2 dyn cm^{-2}). One sees two-layer estuarine flows occurring throughout the harbor: in the Narrows, near the mouths of Jamaica Bay and all four rivers and in most regions of Raritan Bay. The surface-to-bottom salinity difference is about 1‰ in most parts of the harbor, but exceeds values of 2‰ in particular places closed to freshwater sources.

On 16 August (Fig. 5b), winds became south-southeastward and fairly strong ($\approx$1 dyn cm^{-2}). The surface current in Raritan Bay responds quickly and turns from an eastward flowing to a southward flowing direction, and there is a corresponding compensating northward flowing bottom current. In Raritan Bay salinity contours pack closer together at the southern shore. Along the Ambrose Channel bottom high-salinity water is seen to intrude farther north into the es-

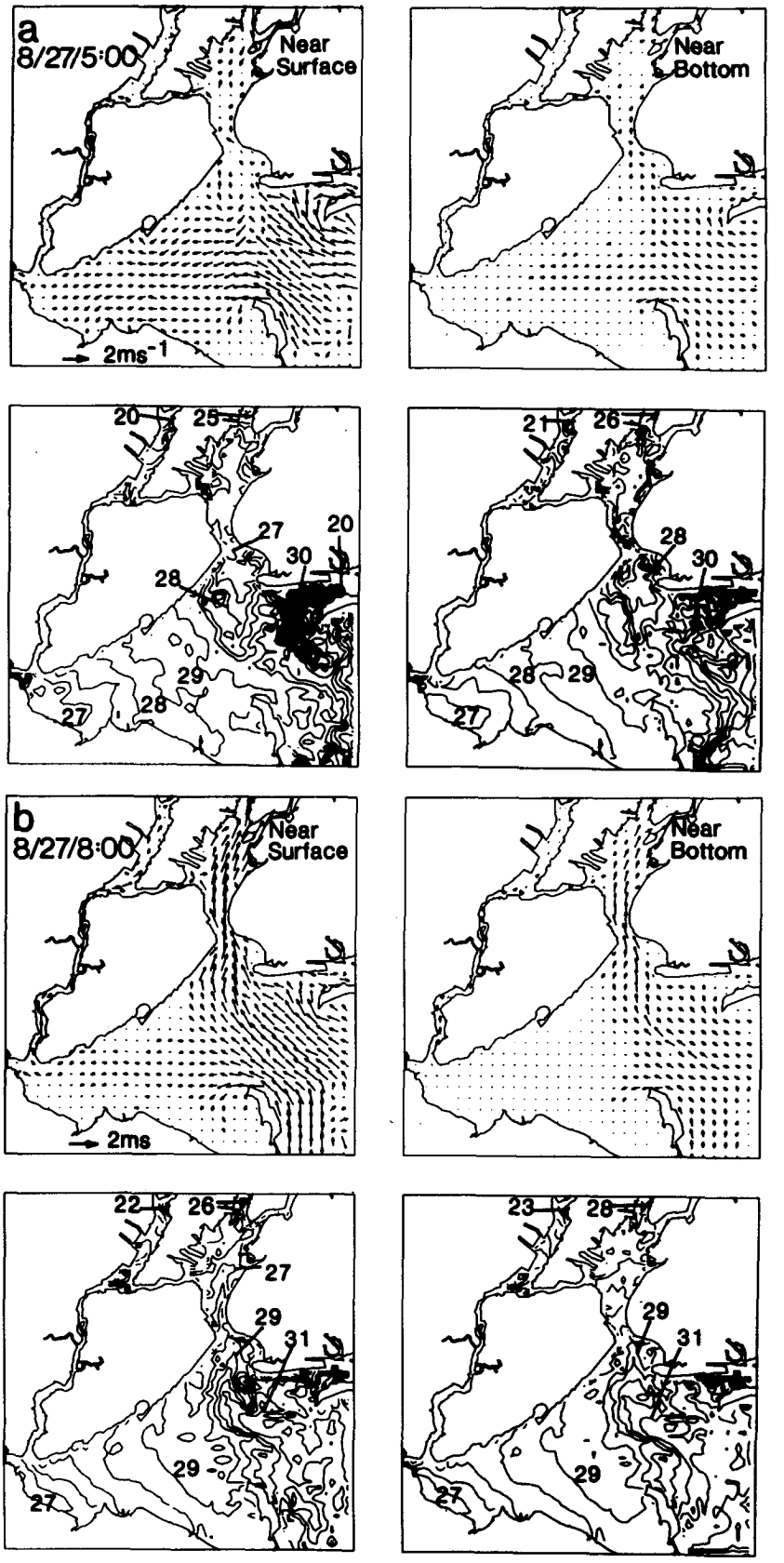

FIG. 4. Computed surface and bottom (one meter from the bottom) velocity vector and salinity contour plots when the vertically integrated current at the Narrows is approximately at (a) slack before flood, (b) 3 hours later, (c) slack before ebb, and (d) 3 hours later. Arrows are plotted at every other grid points. The large salinity contrast emanating from Jamaica Bay is a sewage plume. Time is EST.

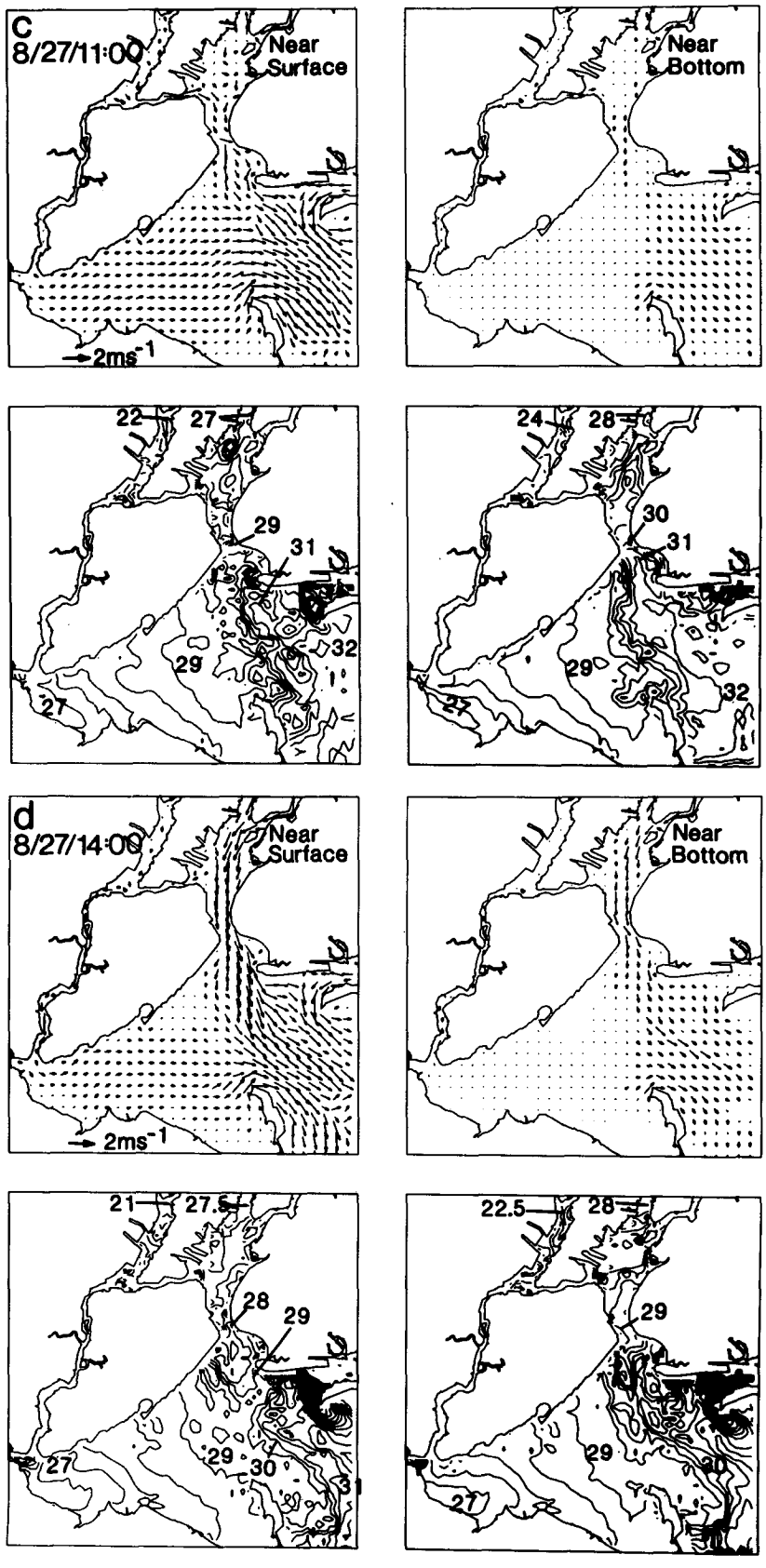

FIG. 4. (*Continued*)

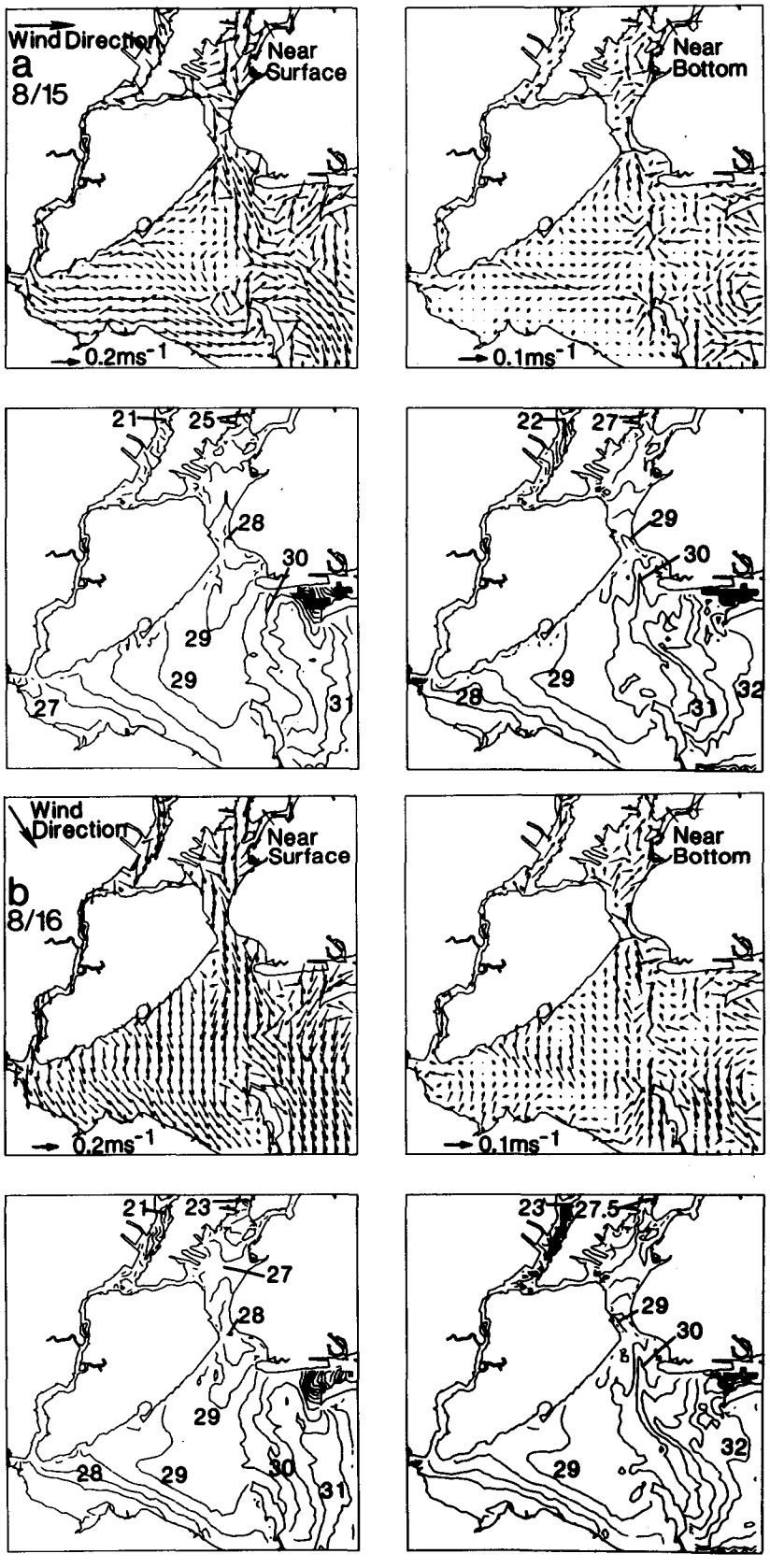

FIG. 5. Computed 25-hour average of surface and bottom velocity vectors and salinity contours centered at 1700 GMT on (a) 15; (b) 16; (c) 18 and (d) 22 August. Average wind direction for each period is also shown. Arrows are plotted at every other grid point.

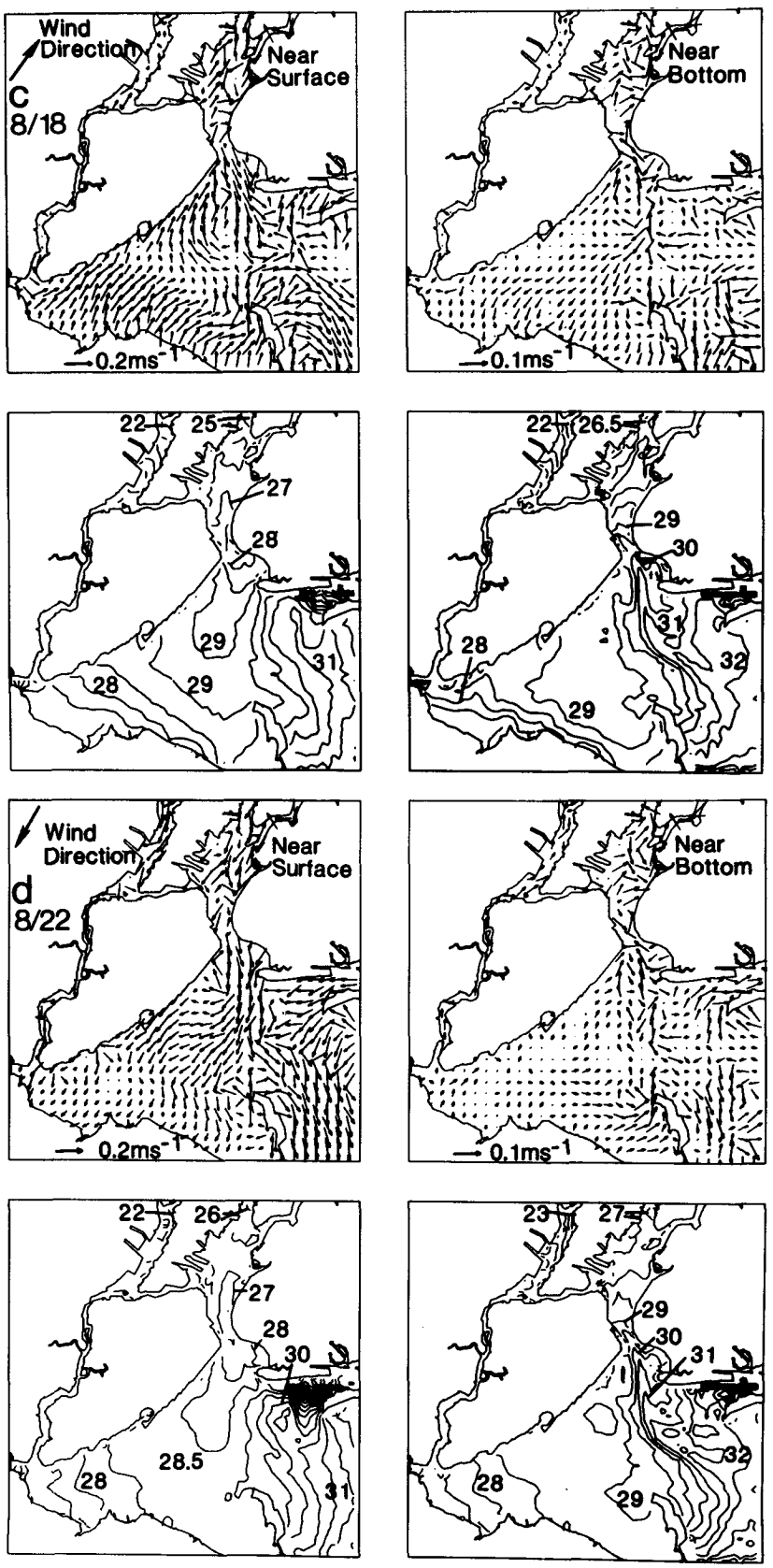

FIG. 5. (*Continued*)

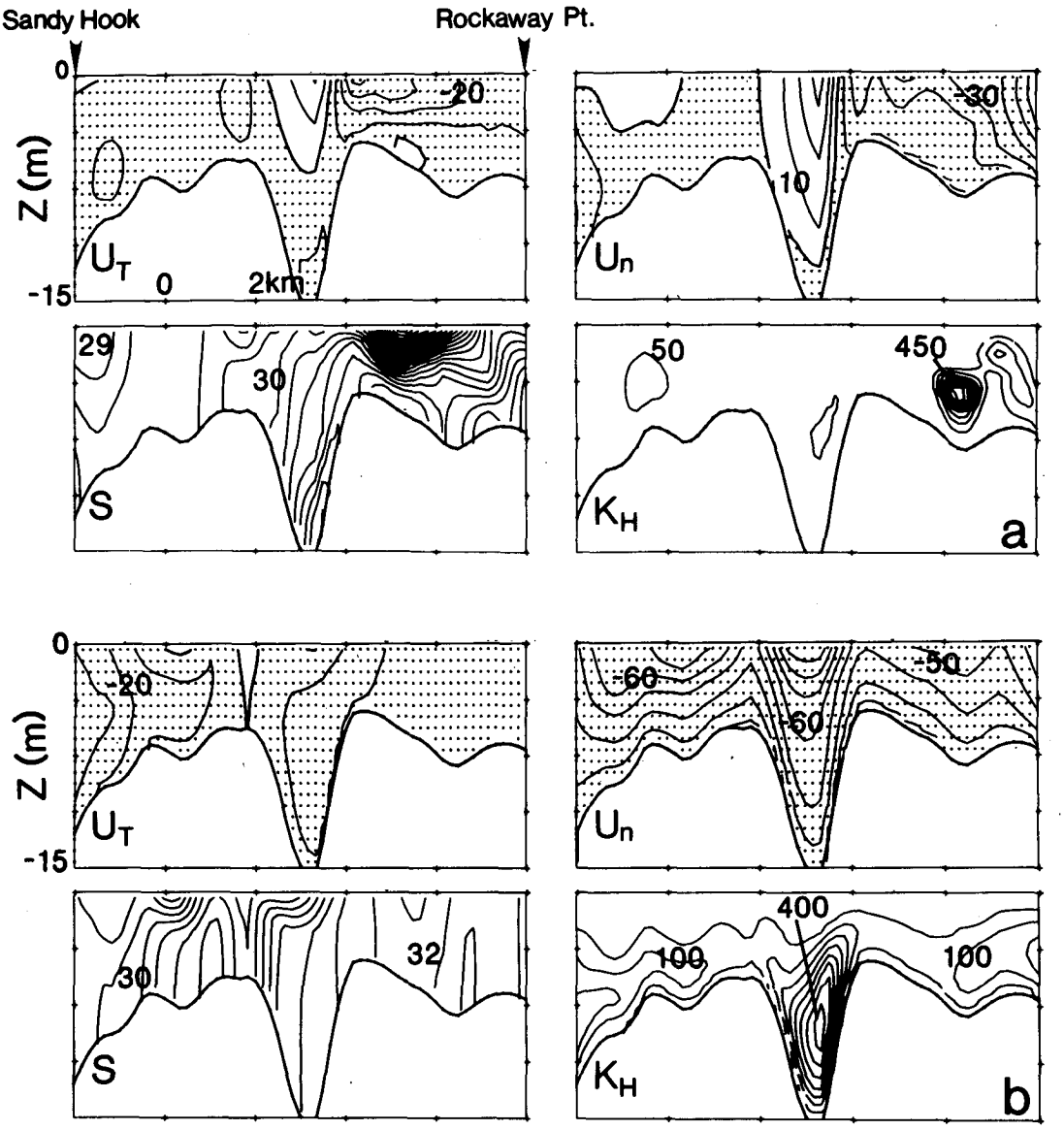

FIG. 6a. Computed contours at 0300 GMT, near the beginning of flood, 20 August 1980 of the velocity U_T (positive to the right) and the normal velocity U_n (positive ebbing), both in cm s^{-1}, the salinity S in ppt and the turbulence mixing coefficient K_H for salt in cm^2 s^{-1} at the Sandy Hook–Rockaway Point transect. The contour intervals are: 10 cm s^{-1} for U_T and U_n, 0.25‰ for S and 50 cm^2 s^{-1} for K_H. Regions of negative U_n and U_T are stippled.

FIG. 6b. Contours at 0600 GMT 20 August.

tuary, driven now by a stronger, two-layer gravitational flow in response to the southward wind.

On 18 August (Fig. 5c), winds became weak (≈0.2 dyn cm^{-2}) and north-northeastward. Currents in Raritan Bay again responded rapidly and the salinity has also relaxed back to its original distribution, shown in Fig. 5a. The response in deeper regions is slower. For example, note that a short surface tongue of 29‰, just south of the Narrows in Fig. 5a, has now elongated farther southward and that the bottom high-salinity water in Ambrose Channel has intruded farther north into the estuary, both in response to the strong southward wind two days previously.

Winds remained light and north-northeastward until 20–23 August (Fig. 5d) when they became southwestward and stronger (≈0.5 dyn cm^{-2}). The salinity in Raritan Bay became more homogeneous vertically and axially (east–west) and the current structure changed to a "reversed" two-layer circulation, with landward surface and seaward bottom flows. The increase in turbulent mixing will be shown to be caused by unstably stratified water columns induced by the up-estuary (the

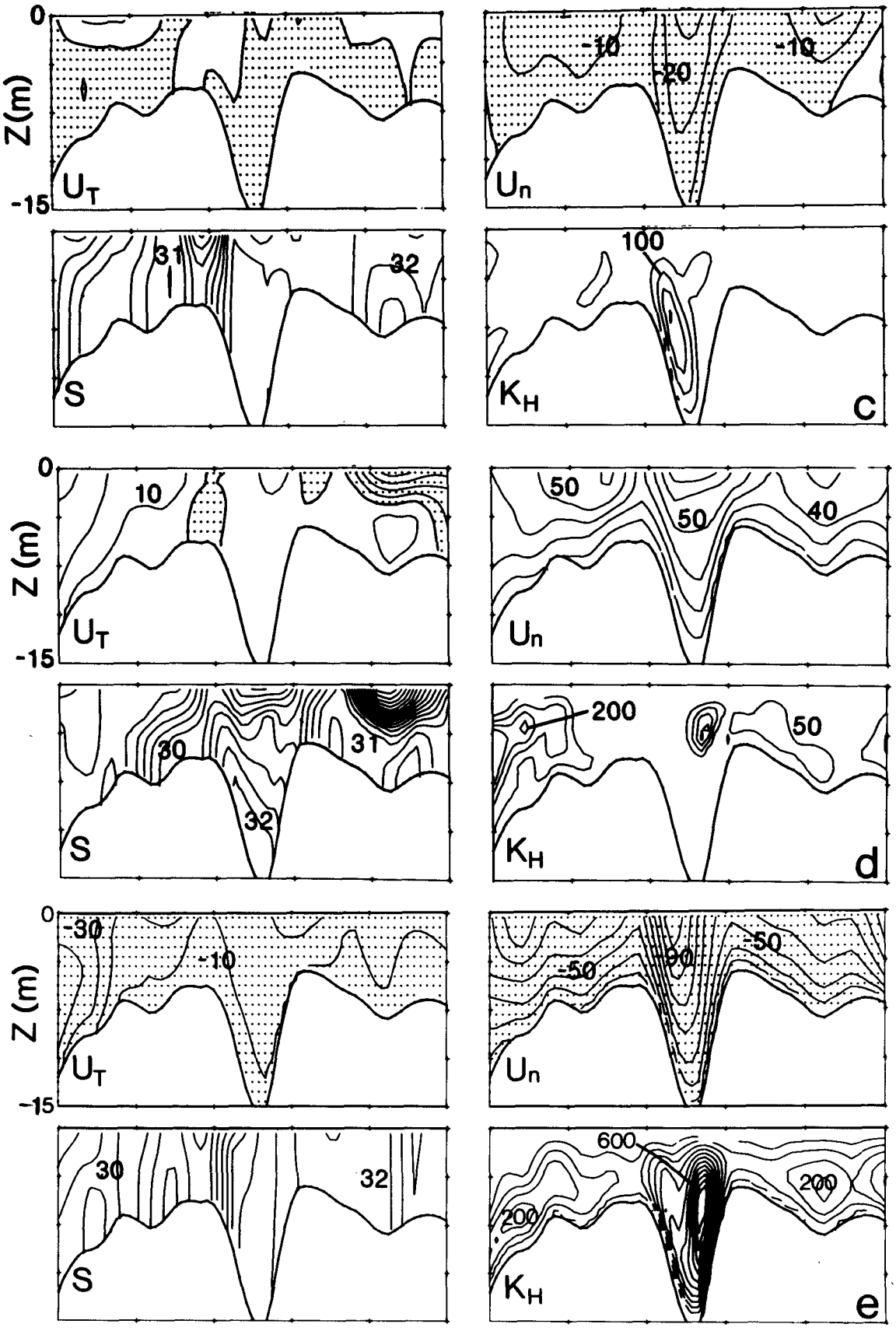

FIG. 6c. Contours at 0800 GMT near the beginning of ebb at this transect.

FIG. 6d. Contours at 1100 GMT.

FIG. 6e. Contours at 1800 GMT.

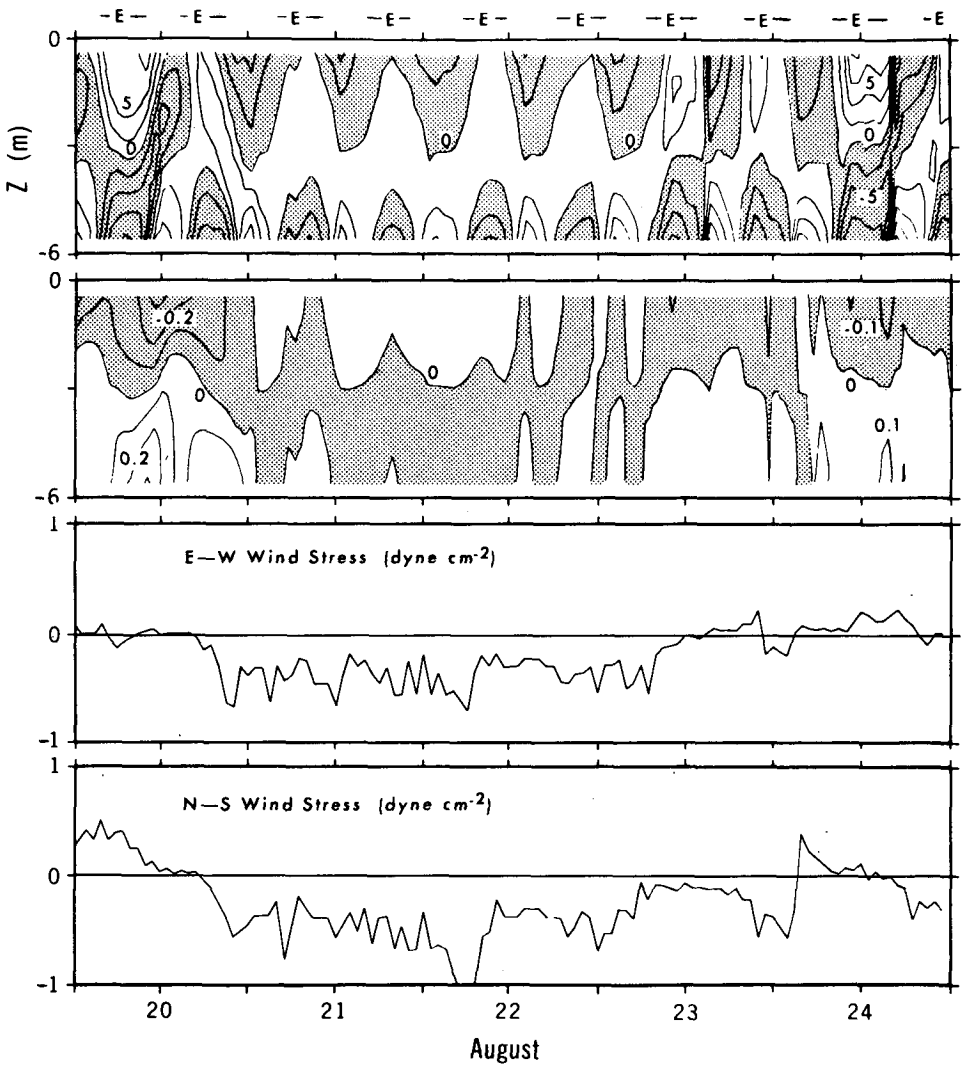

FIG. 7a. Time-depth plots of deviations of velocity (cm s^{-1}, top panel) and salinity (ppt, second panel from top) from their vertical averages in the midposition of a cross section in Raritan Bay (Fig. 1). Ebbing periods are marked by the letter "E" on the top of the figure. The axial (east-west) wind stress (third panel from top) and the cross-channel (north-south) wind stress (bottom panel) in dyn cm^{-2} are also shown. Time is EST.

westward) wind. Note again the up-estuary intrusion of bottom saline (32‰) water along the Ambrose Channel and also the formation of a new tongue of less-saline (28.5‰) water just south of the Narrows.

c. *Temporal variations of U, S and K_H at SHRP transect*

A better understanding of vertical mixing and transverse and vertical variations of velocity and salinity is obtained by studying model results in a number of vertical cross sections in the estuary. The study should provide insight into various mechanisms for salt balance in the estuary, an important topic to be discussed in Part III. The particular cross section we have chosen as an example is the SHRP transect shown in Fig. 6 as a series of instantaneous tangential velocity, normal velocity, salinity and turbulence mixing coefficient contours for one tidal period. The tidal cycle chosen for examination, 19–20 August, was during a neap tide period when vertical stratification was most pronounced.

Figure 6a shows the fields at 0300 GMT 20 August, which corresponds closely to the beginning of flood at SHRP transect. Flood (negative U_n) begins first on the Rockaway Point side of the transect, reaching a value of -60 cm s^{-1}. At the deep midsection channel (the Ambrose Channel) and on the Sandy Hook side of the transect, ebb (positive) currents still prevail near the surface, and flood currents already appear near the bottom. This may be evidence for a weak density-driven flow, especially at the Ambrose Channel, but could also be due to bottom frictional effects: near-

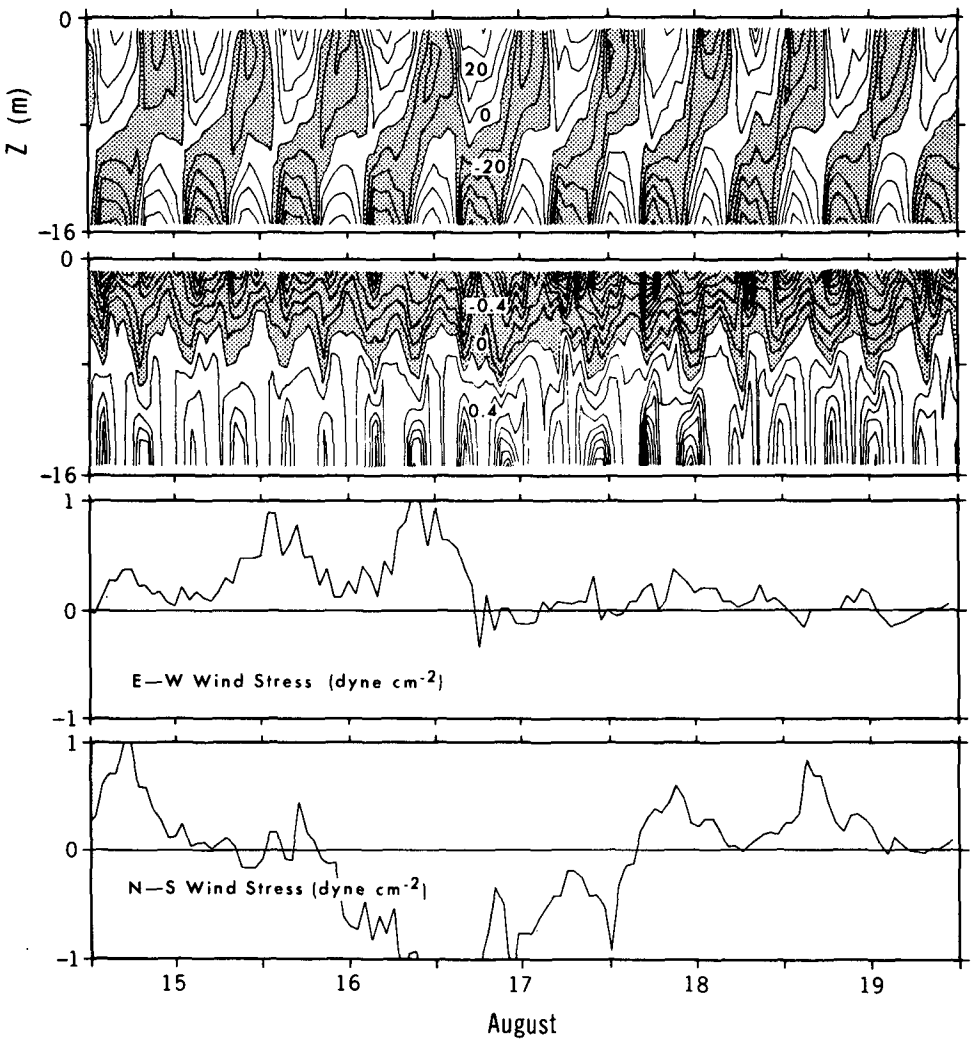

FIG. 7b. As in Fig. 7a but now at a midposition of the cross section in the Narrows (Fig. 1) covering a different period of the up-estuary wind event.

bottom boundary layer fluid with less momentum reverses first under an opposing pressure gradient (cf. Proudman, 1953). Cross-channel velocities U_T (positive to the right) are of the same order as U_n, implying significant flow curvature and hence large centripetal acceleration (Doyle and Wilson, 1978). More saline water is on the right-hand bank (looking landward) and less saline water on the left bank. There is a strong stratification near the surface at the right half of the transect, which is produced by sewage discharge from Jamaica Bay during the previous ebb. Large values of K_H are found near middepth at the right half of the transect. This large turbulent mixing is produced by unstable stratification, $\rho_z > 0$, rather than by vertical velocity shears, which are small at this instant. A detailed study of the instantaneous contours of

$$\mathrm{Ri} = -g\rho_z/\rho_0[(U_z)^2 + (V_z)^2]$$

indicated that this unstable stratification repeats itself at the beginning of each flood tide and is caused by denser water flowing across the transect near the Rockaway Point from a shallow, open-ocean region northeast of the Rockaway Point, overlaying less dense water from Jamaica Bay. There are two ways in which our model gives large mixing when Ri becomes negative. First, there are buoyancy terms in Eq. (10) for $q^2/2$ and q^2l that become "sources" rather than "sinks" when Ri is negative. Secondly, there are stability factors S_M and S_H that increase by factors of 2–5 from their neutral values corresponding to zero stratification case. Neutral values for K_M and K_H are about 2.5×10^{-3} HU_d, where U_d is the depth-mean amplitude of the current (Fischer *et al.*, 1979, p. 250), and are about 150 $\mathrm{cm^2\ s^{-1}}$ for the right-hand side of the transect. Therefore, a maximum of about three times this neutral value of K_H is calculated by the model. For later reference we shall refer to this type of instability as a density advection instability.

At 0600 GMT 20 August (Fig. 6b), full flooding velocity developed across the section and turbulent mixing is mainly due to an almost 3-fold increase in turbulence kinetic energy (not shown), produced by large velocity shears. However, density advection instability is still evident in the midsection region, where Ri attains a minimum value of -0.05 and values of K_H greater than its neutral value of about 350 are found. The water becomes more vertically homogeneous as shown by the salinity contours.

At the beginning of ebb (0800 GMT, Fig. 6c) bottom currents on both sides of the transect are ebbing while near-surface currents are still flooding. This is due to bottom frictional effect since for the present low-discharge simulation, horizontal density gradients are too weak to sustain a bottom flooding flow during the turn of ebb. Turbulent mixing is primarily produced by vertical velocity shears. Salinity contours are displaced leftward by the (previously) large flood currents in the deep channel.

Full ebb currents develop at 1100 GMT (Fig. 6d) with low salinity values seen near the surface. Less-saline sewage water from Jamaica Bay is clearly seen near the right-hand bank where the cross-channel surface velocity is negative. There is a surface jet with velocity greater than 0.7 m s^{-1} above the Ambrose Channel. Despite the large velocity shears, turbulent mixing is inhibited by strong stratification in most parts of the section, and only becomes more intense near the left-hand bank, where Ri $\approx$ 0.05.

The subsequent tidal cycle (1500–0300 GMT 20–21 August) with larger tidal range caused by diurnal tidal inequality produces more mixing and less stratification. Figure 6e shows contours at about two hours before the end of flood at 1800 GMT 20 August and can be compared with Fig. 6b.

4. Discussion

Density advection instabilities that we have found in the model calculation occur during times of slack water and also during the flood stage. Examples were given in Fig. 6a, b. This intense mixing generally lasts for about 1–2 hours and there should be ample time for measurements in a field program. In Part II, we shall describe observations at the SHRP transect that verify the model's predictions. Observations made by Bowden *et al.* (1959) in Red Wharf Bay, North Wales, show eddy viscosity values in the range of 400–600 cm^2 s^{-1} during the first two hours of flood current. These values are larger than the neutral value of about 248 cm^2 s^{-1} at the site of the experiment (see their Table 2 and p. 301). The corresponding results for ebb current are less certain since observed values appear to be close to the neutral value of about 221 cm^2 s^{-1}. These observations are consistent with our model results, which suggest that, during flood, denser water tends to override lighter water, if only momentarily, and intense mixing is produced. This type of mixing is different from that caused by the breaking of long internal waves unable to travel upstream against maximum ebb currents, observed in the Duwamish River, a salt wedge estuary, by Partch and Smith (1978). In that case, Ri was always positive and K_H was small with maximum value reaching only 6 cm^2 s^{-1}.

Density advection instabilities can also be produced by "up-estuary" wind events. Theoretical studies using similarity methods (Rattray and Hansen, 1962; Hansen and Rattray, 1965) and somewhat more general perturbation analysis (Oey, 1984) suggest that wind stress in the direction of surface ebb currents increases stratification while an opposing wind stress would decrease the surface-to-bottom salinity difference and, if the wind were strong enough, would destabilize the water column. The analytical solution is not valid in the destabilization state, however, since the assumption of constant eddy coefficients, for example, would break down under such a condition. Our simulation results confirm the theoretical inferences as we illustrate in Fig. 7a for a midstation in Raritan Bay, where tidal currents are weak and effects of wind more pronounced. The figure shows time-depth plots of deviations of (east–west component of) velocity and salinity from their depth-averaged values. Unstable layers are seen therefore as positive salinity deviation overlying negative (shaded) deviation. Periods of such unstable events occurred from 1700 GMT 20 August through 23 August when there was a westward (up-estuary) wind. Large mixing results as discussed previously in conjunction with Fig. 5d, with large values of K_M and K_H of the order of 100 cm^2 s^{-1}, 2–3 times larger than their neutral values of about 40 cm^2 s^{-1} in Raritan Bay. Theoretical analysis also gives the effect of wind as a dimensionless parameter proportional to the ratio of the wind stress to the vertical eddy coefficient. Thus, in regions of the estuary where tidal currents are strong, wind-induced, density advection instabilities should not occur. We illustrate this in Fig. 7b for a station in the Narrows (where neutral K_H and K_M values are about 350 cm^2 s^{-1}). Up-estuary (northward) winds from 1700 GMT 14 August through 1300 GMT 15 August, and from 2000 GMT 17 August through 1000 GMT 20 August had little effect on density stratification, and the flow was stably stratified throughout these periods.

Theoretical analysis also predicts increased gravitational flow with down-estuary wind. This was discussed in conjunction with our numerical results shown in Fig. 5, but is illustrated here more clearly in Fig. 8, which shows low-pass filtered time-depth plots of salinity and velocity at a midstation in the SHRP transect. Both increased stratification and gravitational circulation are seen as responses to a down-estuary wind on 16 and 17 August.

Another important aspect of time-dependent tidal mixing is caused by diurnal tidal inequality illustrated previously in conjunction with Figs. 6b and 6e. The

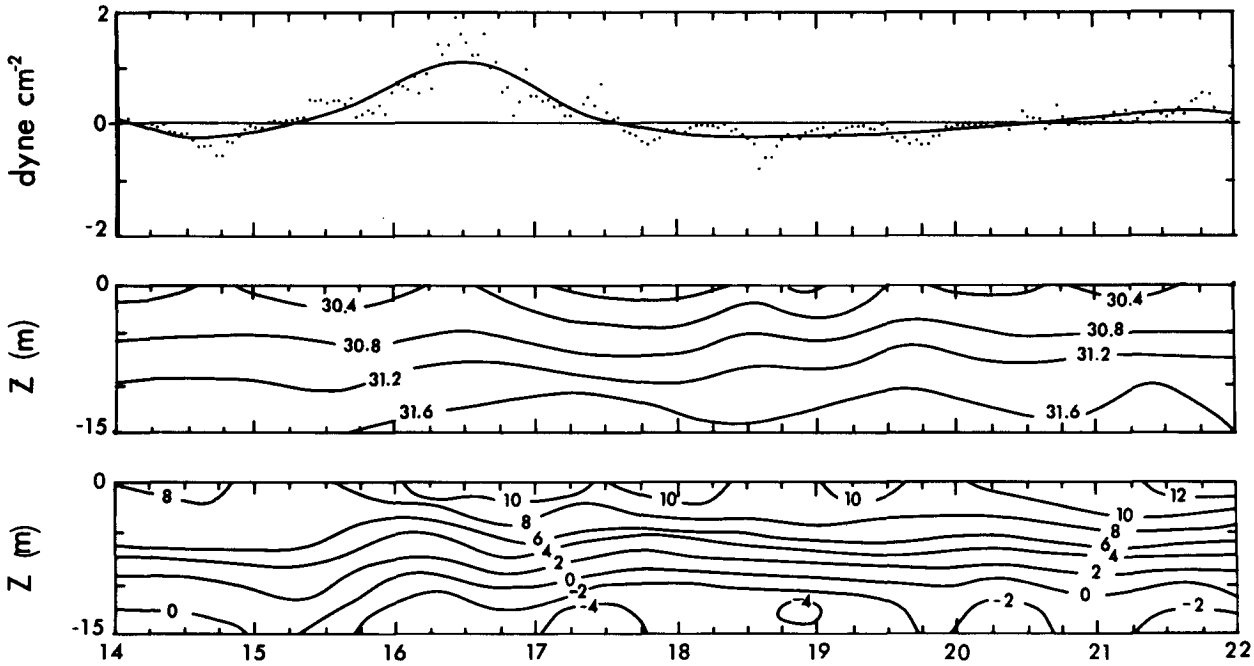

FIG. 8. Time-depth contour plot of low-pass filtered velocity (bottom panel, cm s^{-1}, positive ebbing) and salinity (middle panel, ppt) at a midstation at the Sandy Hook–Rockaway Point transect for 14–22 August 1980 (Time: EST). Both the original and low-passed wind stress components (positive down-estuary or seaward) normal to the transect are also shown in the top panel.

difference in V_T, the tidal rms velocity, between the two tidal cycles is only 10 cm s^{-1}, and it may seem surprising that such a small change can bring about large differences in eddy mixing in the estuary. Fischer (1976) noted that $\mathrm{Ri}_E = H/L_E$ is a measure of stratification in estuaries, where $L_E = V_T^3/(gu_f \Delta\rho/\rho)$ is a measure of "estuarine Monin-Obukhov" length scale, $\Delta\rho$ is the density difference between the ocean water and freshwater and u_f is freshwater discharge velocity. Because of the cubic power in V_T, Ri_E and hence the turbulent mixing are sensitive to small variations in V_T.

5. Conclusion

Using observed sea levels, winds, and river and sewage discharges, we have numerically simulated the time-dependent, three-dimensional velocity and salinity structures in the Hudson–Raritan estuary for the period July–September 1980. Results of the simulation have given new insights into the physical processes involved in the circulation and mixing of a partially mixed estuary. Computed salinity contours show small-scale (3 km × 3 km × 10 m), three-dimensional eddies that are produced by interaction of the time-dependent velocity and density fields with coastline and bottom bathymetry, and which are advected and subsequently mixed throughout the vertical water columns. These are important physical processes that contribute to shear dispersion in an estuary.

In addition to turbulence produced by shearing tidal and/or wind-induced currents, density advection instabilities contribute to mixing processes in an estuary. Such a mixing mechanism was first suggested by Rattray and Hansen (1962) from analytical response solutions to up-estuary wind in an idealized, steady-state, two-dimensional (depth and axial) estuary. Our simulation extends their results to the time-dependent, three-dimensional case. Moreover, we showed that density advection instabilities can occur even in the absence of winds, and are caused by differential advection of density fields by the three-dimensional velocity field. This finding is consistent with observations by Bowden *et al.* (1959).

Unsteady winds are important in changing the vertical velocity and salinity structures, which in turn change the turbulent mixing in the estuary and would therefore affect up-estuary salt transports. Both the two-dimensional horizontal circulation and the vertical gravitational-induced circulation vary considerably with wind forcing at subtidal time scales. For the rather light wind stress ($\approx$0.5 dyn cm^{-2}) during the simulation period, subtidal variations in velocity and salinity fields are most significant in Raritan Bay where tidal currents are weak.

Acknowledgments. We wish to thank Susan Salyer for preparing the manuscript. Thanks also to an anonymous referee who reviewed all three parts of this series of papers and gave many valuable comments. Drs. A.

Blumberg and K. Bryan read the first draft of the manuscript and gave many valuable comments. The figures were drafted by P. Tunison and processed by J. Conner. Anna Boyette and Suzanne McIntosh prepared the final version of the figures. This research was sponsored by the New Jersey Sea Grant Program under a grant from the Office of Sea Grant of NOAA, Grant 81 AA-D-0065, Project R/E-3. Additional funding was provided under Grant NA 80 RAD 00033 from the Northwest Office of the Office of Marine Pollution Assessment of NOAA. LYO was supported in part by the Visiting Scientist Program of Princeton University/ NOAA, Grant 04-7-022-44017.

REFERENCES

Ayers, J. C., B. H. Ketchum and A. C. Redfield, 1949: Report to Middlesex County Planning Board on hydrographical considerations relative to the location of sewer outfalls in Raritan Bay. Tech. Rep. Ref. No. 49-13, WHOI, 41 pp.

Blumberg, A. F., and G. L. Mellor, 1980: A coastal ocean numerical model. *Lecture Notes on Coastal and Estuarine Studies,* J. Sundermann and K. P. Holz, Eds., Springer-Verlag, 265 pp.

——, and ——, 1983: Diagnostic and prognostic numerical circulation studies of the South Atlantic Bight. *J. Geophys. Res.*, **88,** 4579–4592.

Bowden, K. F., L. A. Fairbairn and P. Hughes, 1959: The distribution of shearing stresses in a tidal current. *Geophys. J. Roy. Astron. Soc.*, **2,** 288–305.

Bunker, A. F., 1976: Computation of surface energy flux and annual air–sea interaction cycles of the North Atlantic Ocean. *Mon. Wea. Rev.*, **104,** 1122–1139.

Caponi, E. A., 1976: The simulation of estuarine circulations with a fully three-dimensional numerical model. *Estuarine Processes, Vol. 2,* M. Wiley, Ed., Academic Press, 332–346.

Chatwin, P. C., 1976: Some remarks on the maintenance of the salinity distribution in estuaries. *Estuarine Coastal Mar. Sci.*, **4,** 555–566.

Doyle, B. E., and R. E. Wilson, 1978: Lateral dynamic balance in the Sandy Hook to Rockaway Point transect. *Estuarine Coastal Mar. Sci.*, **6,** 165–174.

Festa, J. F., and V. H. Hansen, 1976: A two-dimensional model of estuarine circulation: The effects of altering depth and river discharge. *Estuarine Coastal Mar. Sci.*, **4,** 309–323.

Fischer, H. B., 1976: Mixing and dispersion in estuaries. *Annual Review of Fluid Mechanics,* Vol. 8, Annual Reviews, 107–133.

——, E. J. List, R. C. Y. Koh, J. Imberger and N. H. Brooks, 1979: *Mixing in Inland and Coastal Waters.* Academic Press, 483 pp.

Fofonoff, N. P., 1962: Physical properties of sea-water. *The Sea,* Vol. 1, Wiley-Interscience, 3–30.

Hamilton, P., 1975: A numerical model of the vertical circulation of tidal estuaries and its application to the Rotterdam waterway. *Geophys. J. Roy. Astron. Soc.*, **40,** 1–21.

Hamrick, J. M., 1979: Salinity intrusion and gravitational circulation in partially stratified estuaries. Ph.D. thesis, University of California, Berkeley, 451 pp.

Hansen, D. V., and M. Rattray, 1965: Gravitational circulation in straits and estuaries. *J. Mar. Res.*, **23,** 104–122.

Johns, B., 1978: The modeling of tidal flow in a channel using a turbulence energy closure scheme. *J. Phys. Oceanogr.*, **8,** 1042–1049.

Leendertse, J. J., and S. K. Liu, 1977: A three-dimensional turbulent energy model for nonhomogeneous estuaries and coastal sea systems. *Hydrodynamics of Estuaries and Fjords, Proc. Ninth Leige Colloq. Ocean Hydrodyn.*, C. J. C. Nihoul, Ed., Elsevier, 387–405.

Mellor G. L., and T. Yamada, 1974: A hierarchy of turbulence closure models for planetary boundary layers. *J. Atmos. Sci.*, **31,** 1791–1806.

——, and ——, 1977: Corrigenda. *J. Atmos. Sci.*, **34,** p. 1482.

——, and ——, 1982: Development of a turbulence closure model for geophysical fluid problems. *Rev. Geophys. Space Phys.*, **20,** 851–875.

Oey, L.-Y., 1984: On steady salinity distribution and circulation in partially mixed and well mixed estuaries. *J. Phys. Oceanogr.*, **14,** 629–645.

——, G. L. Mellor and R. I. Hires, 1985a: Tidal modeling of the Hudson-Raritan estuary. *Estaurine Coastal Shelf Sci.*, **20,** 511–527.

——, G. L. Mellor and R. I. Hires, 1985b: A three-dimensional simulation of the Hudson-Raritan estuary. Part II: Comparison with observation. *J. Phys. Oceanogr.*, **15,** 1693–1709.

——, ——, and ——, 1985c: A three-dimensional simulation of the Hudson-Raritan estuary. Part III: Salt flux analyses. *J. Phys. Oceanogr.*, **15,** 1711–1720.

Owen, A., 1980: A three-dimensional model of Bristol channel. *J. Phys. Oceanogr.*, **10,** 1290–1302.

Partch, E. N., and J. D. Smith, 1978: Time dependent mixing in a salt wedge estuary. *Estuarine Coastal Mar. Sci.*, **6,** 3–19.

Proudman, J., 1953: *Dynamical Oceanography.* Methuen/Wiley, 409 pp.

Rattray, M., Jr., and D. V. Hansen, 1962: A similarity solution for circulation in an estuary. *J. Mar. Res.*, **20,** 121–133.

Sundermann, J., and W. Lenz, 1983: *North Sea Dynamics,* Springer-Verlag, 693 pp.

Swansen, R. L., 1976: *Tides.* Mesa New York Bight Atlas Monogr. 4, New York Sea Grant Institute, 33 pp.

Taylor, G. I., 1954: The dispersion of matter in turbulent flow through a pipe. *Proc. Roy. Soc. London,* **A223,** 446–468.

Tee, K.-T., 1979: The structure of three-dimensional currents. Part I: Oscillating currents. *J. Phys. Oceanogr.*, **9,** 930–944.